1.3
ACP Processing

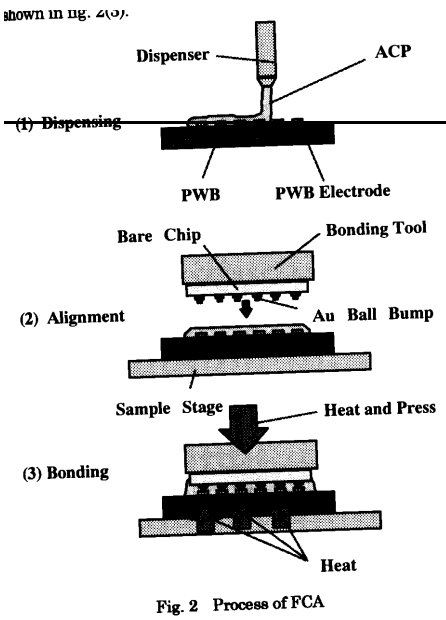

Fig. 2 Process of FCA

Dispensing

- Motomura et al, IEMT/IMC, 1999

Flip-chip Process using ACF
(KAIST)

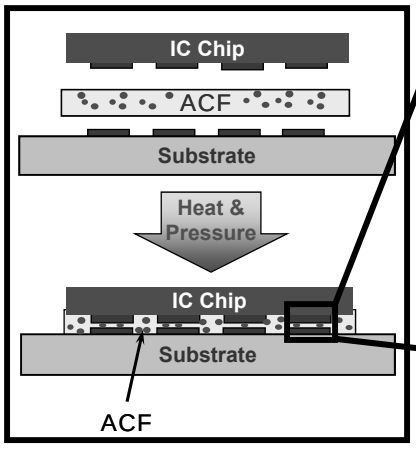

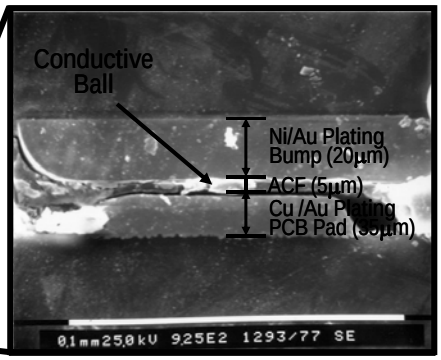

Ni/Au Bump ACF Joint

WLP with Pre-applied ACF [Son et al (KAIST), ECTC'06

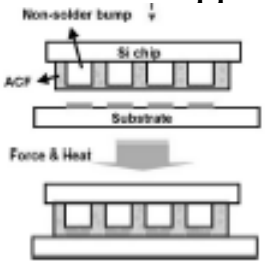

Fig. 1 Schematic diagram of fabrication processes using pre-applied ACFs for flip chip applications

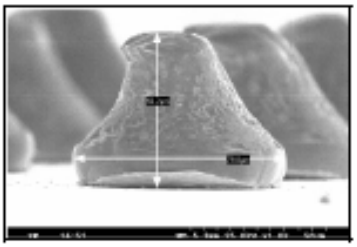

Fig. 2 Au stud bumps of a test chip (60μm height and 80μm diameter)

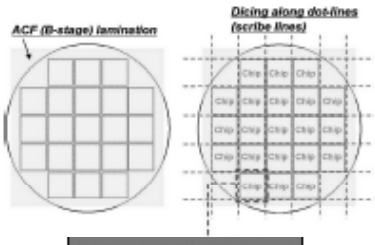

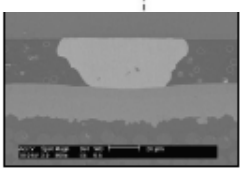

(b)

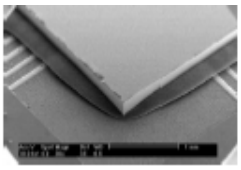

(c)

Fig. 8 (a) Flip chip assembly using ACF WLP, (b) Cross-sectional image of Au stud bump/ACF joints, and (c) ACF fillets formed along the chip edge

ACA: Kim, Jang, Kim, Son, & Paik, Proc. ECTC 2008
Flip-chip assembly (e.g. on ITO) conventionally by ACF→WLP with ACP (ACA solution)
Viscosity increased by conductive & silica particles; high viscosity → voids
Viscosity decreased at higher T → no voids for 50°C print
Dry/outgas at 80°C (no cure for T≤ 80°C)

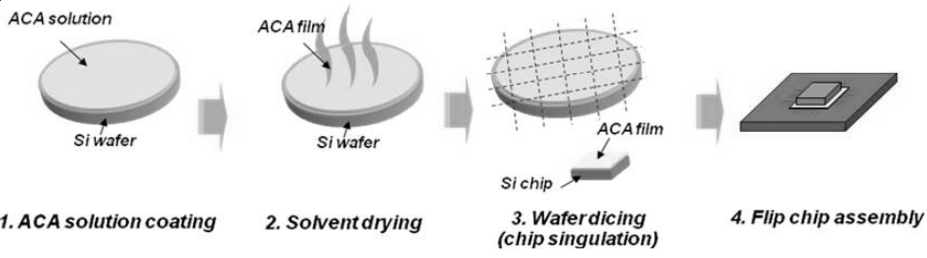

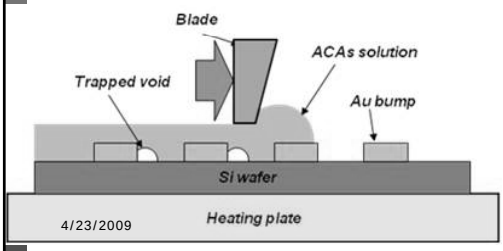

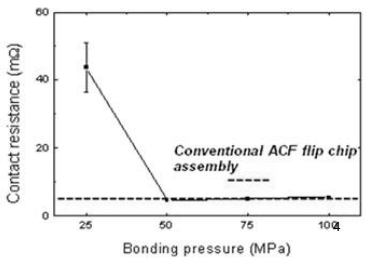

ACA: Kim, Jang, Kim, Son, & Paik, Proc. ECTC 2008

Flip-chip assembly (e.g. on ITO) conventionally by ACF→WLP with ACP (ACA solution)

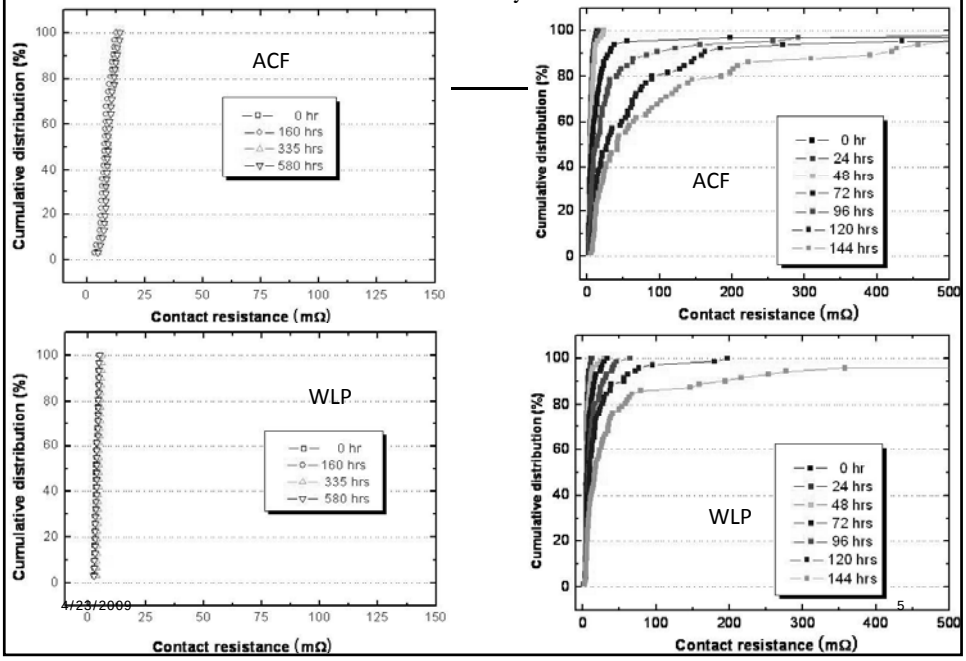

4/23/2009

5

Nagamatsu, Kakiuchi, & Suga Proc. Polytronic 2007

Batch bonding using elastomer

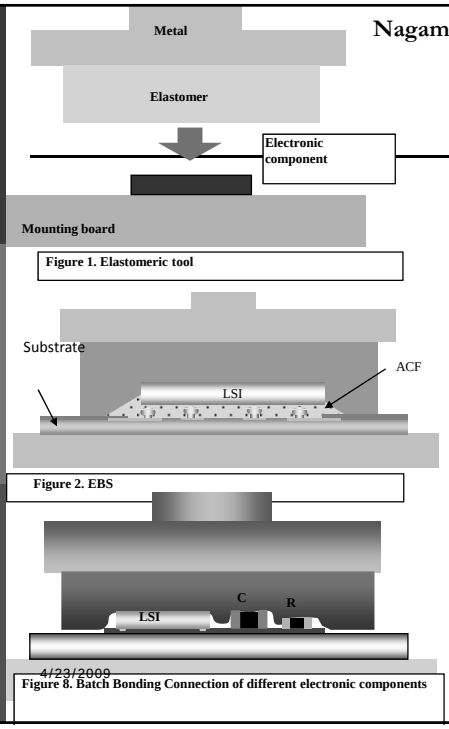

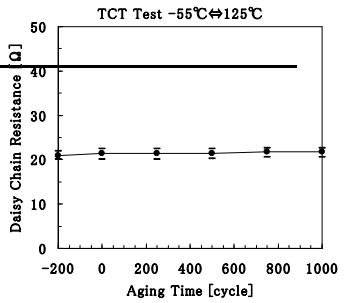

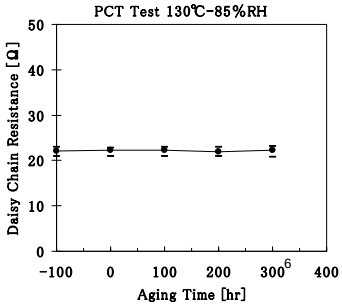

4/23/2009

Figure 8. Batch Bonding Connection of different electronic components

6

Ultrasonic ACF Bonding

[Lee et al (KAIST), ECTC'06

Figure 3. A schematic diagram of the flip chip assembly structure using a jig for TS bonding.

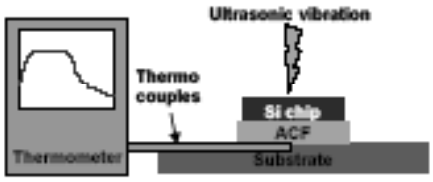

Figure 2. A schematic diagram of in-situ ACF temperature measurement

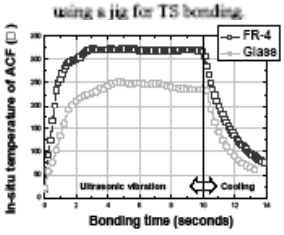

Figure 6. In-situ temperatures of the ACF layer on FR-4 and glass substrates during TS bonding at room temperature.

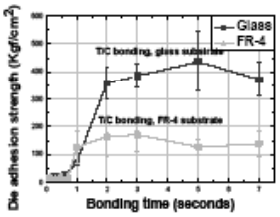

Figure 9. Die adhesion strengths of TS bonded specimens on FR-4 and glass substrates.

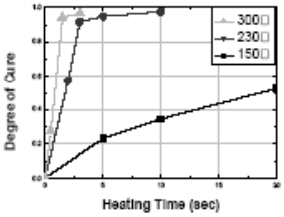

Figure 7. Isothermal cures of ACFs at various curing temperatures.

2.1 Adhesion
NCF flip chip on flex:
Peel strength correlation with degree of cure

(Tan, Chan, & Lui,
IEEE Trans Adv Pkg 29(3) 2006)

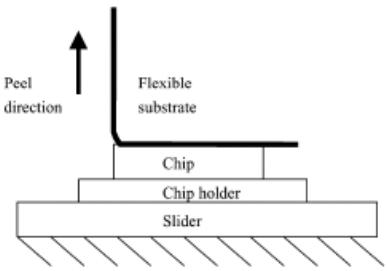

Fig. 3. Peel strength measurement set up.

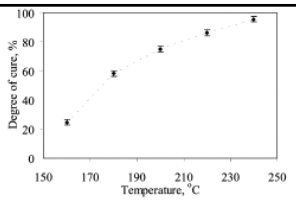

Fig. 5. Degree of cure of NCF bonded under different temperatures with the same bonding time, 10 s.

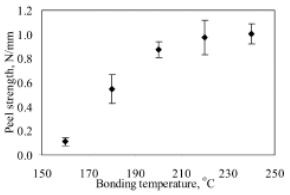

Fig. 6. Peel strength of NCF at different bonding temperatures.

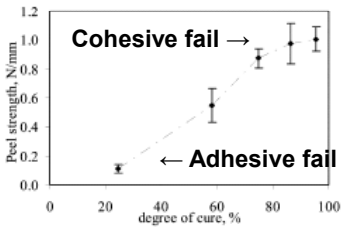

Fig. 8. Peel strength of NCF at different degrees of cure.

Adhesion/shear stress with stress testing: Epoxy variations

(Chen et al, ESTC 2006)

ACF3: snap cure

Table 1 Composition of ACFs

Adhesive	ACF 1	ACF 2	ACF 3
Binder	Thermoset epoxy Bisphenol A type	Thermoset epoxy Bisphenol A type	Thermoset epoxy Bisphenol A type
Curing agent	Phenol + aliphatic diamine	Phenol type	Imidazole system
Conductive particles	Ni/ Au coated plastic ball	Surface treated Ni powder	Ni/ Au coated plastic ball
Diameters of particles	4.8μm	5.3μm	4.8μm
Tg	80°C	130°C	160°C
CTE (ppm/K)	368.1	185.1	117.7

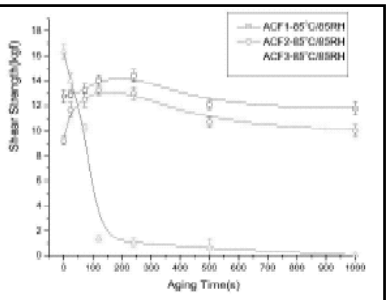

Figure 11. Shear stress of ACFs after 85°C/ 85%R.H. reliability test

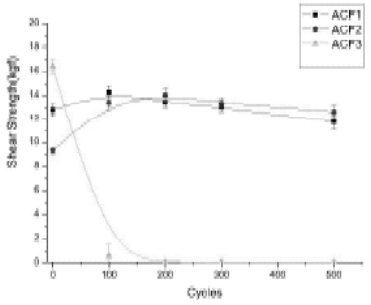

Figure 12. Shear stress of ACFs after thermal cycling test for 500 cycles

Process bubble formation

Kim et al (Paik) ECTC 2006

Surface roughness correlation

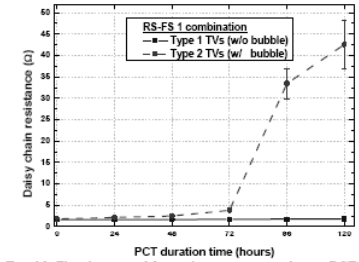

Fig. 10. The changes of daisy chain resistance during PCT.

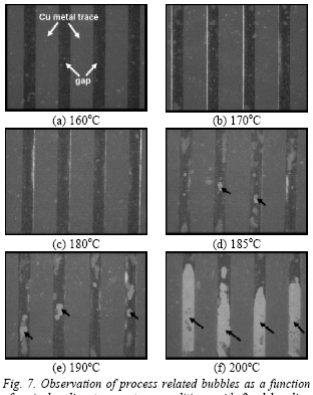

Fig. 7. Observation of process related bubbles as a function of main bonding temperature conditions with fixed bonding pressure at 15.3 MPa. Bubbles appeared only at the TVs of RS-FS 1 combination

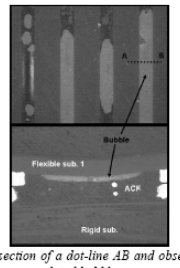

Fig. 8. Cross-section of a dot-line AB and observation of the location of a process related bubble

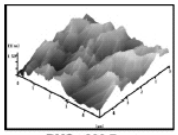

(a) As-received PI

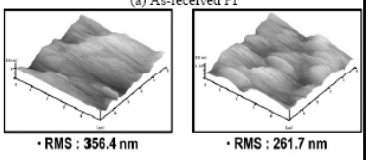

(b) Ar plasma treated PI (c) O_2 plasma treated PI

Fig. 12. Comparisons of PI surface morphologies before and after plasma treatment.

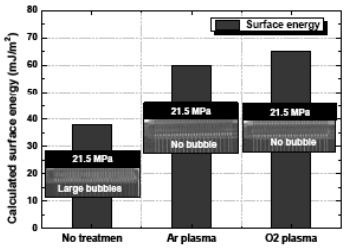

Fig. 13. Comparisons of surface energies and bubbles formation after plasma treatment on FS1 surfaces.

2.3 Ni Particle Deformation with Pressure [Liu et al]

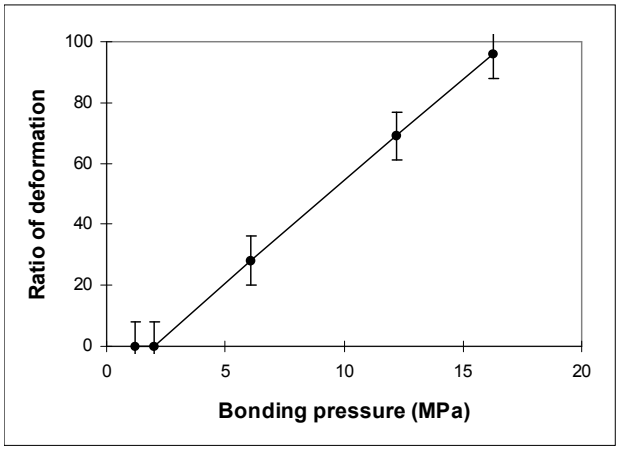

Force-Resistance-Deformation for Rigid & Deformable Particles [Wu et al]

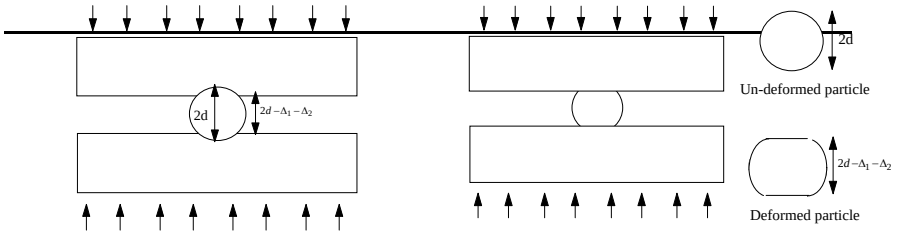

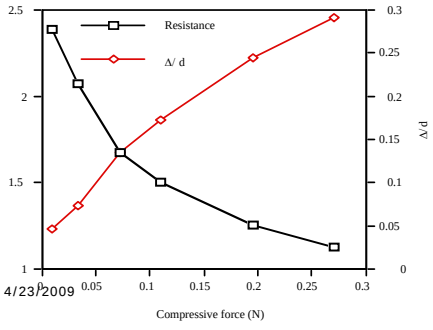

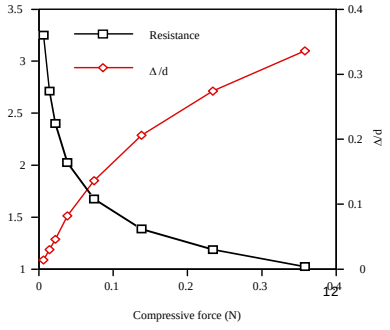

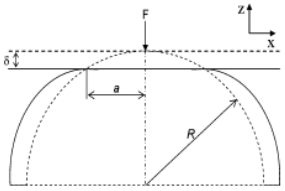

Fig. 2. Schematic deformation of a half conductive particle when a contact load is applied.

Contact area $A = \pi a^2 = \pi g R \delta = g\pi(3FR/4E)^{2/3}$

where (linear elastic) $1 < g < 2$ (fully plastic)

Bonding force	Core type A	Core type B
20N	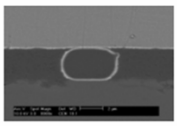	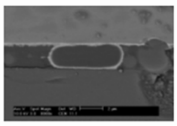
50N	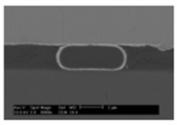	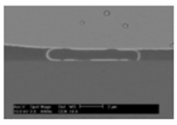
200N		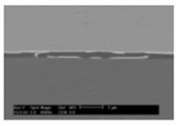

Kwon & Paik, IEEE Trans CPT 2006

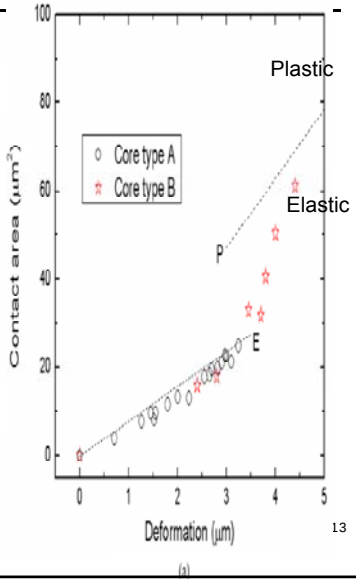

13

2.4. ACA Particle Flow

Adhesive Flow under Pressure [Mannan et al]

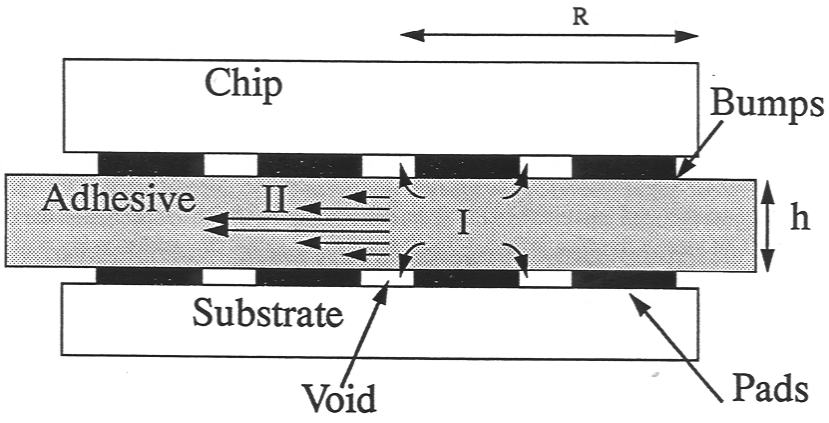

4/23/2009

14

Early flow simulation results [Mannan et al]

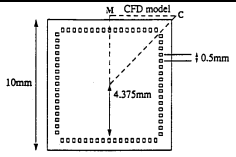

Fig. 3. Sketch of pads at the periphery of the chip and the segment of the chip required for CFD modeling.

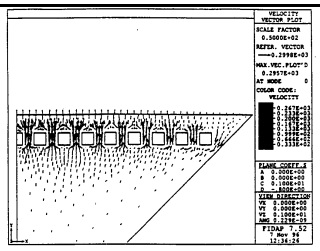

Fig. 4. Flow pattern predicted by CFD around the bumps sketched in Fig. 3.

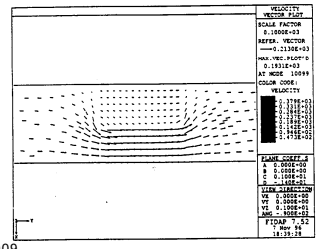

Fig. 10. Flow of fluid over the bumps sketched in Fig. 9 at 500 μm pitch.

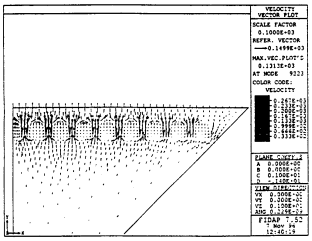

Fig. 5. Flow pattern predicted by CFD over the bumps sketched in Fig. 3.

Flip-Chip Bumps (KSW-Microtec)

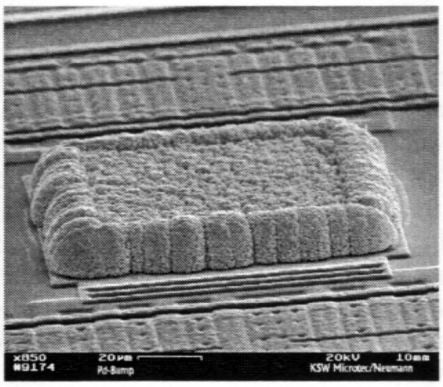

Fig. 3: View of electroless deposited Pd-bump 20µm height patented*) by KSW Microtec

3. ACA Resistance vs No-Pb Solder [Wong, HDP'05]

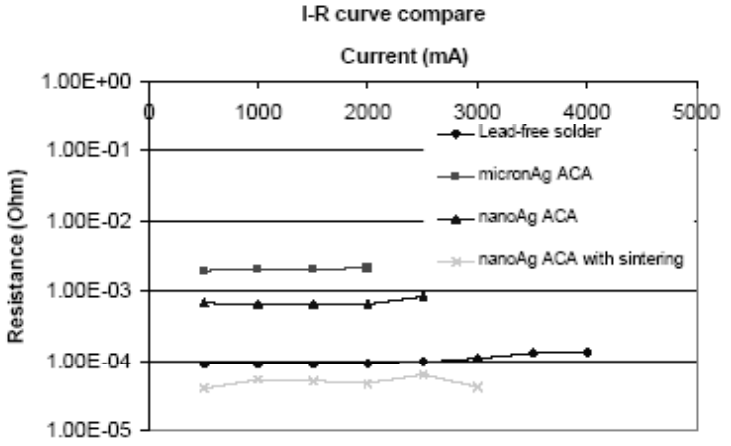

Figure 13 Comparison of current-voltage relationship of different ACAs and lead-free solders

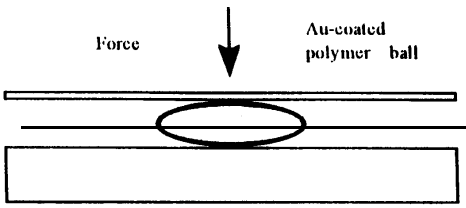

3.1 ACA Conduction Models: Analytical

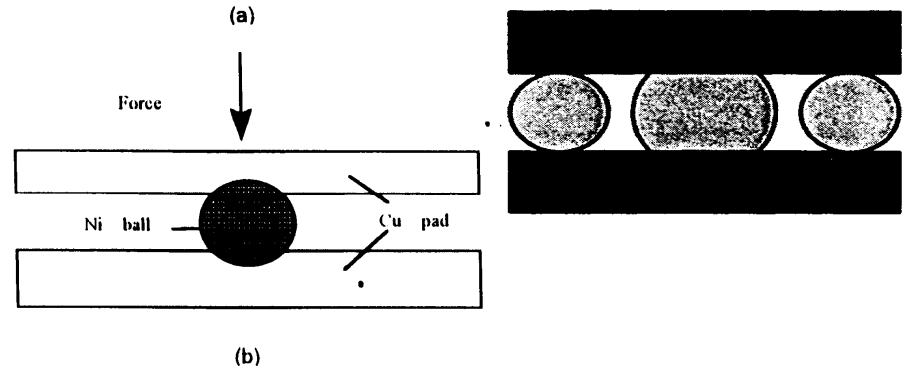

Analytical Prediction & Experiment: Resistance vs Pressure

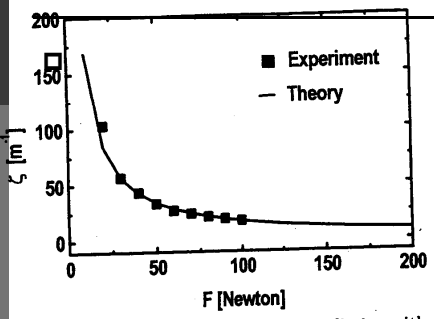

FIG. 3. A comparation of the present prediction with experimental data [5].

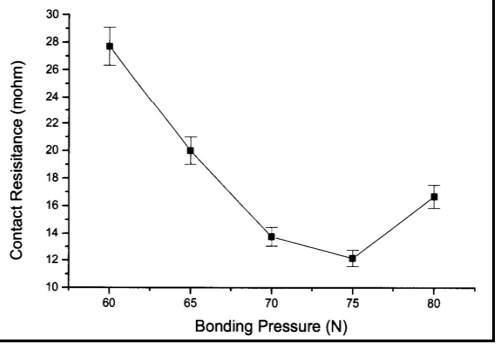

ACA/ACF Electrical Modeling

[Dou et al]

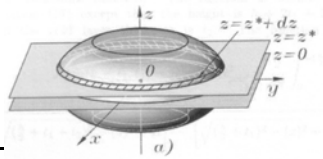

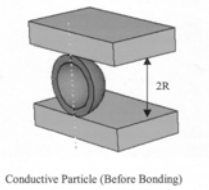

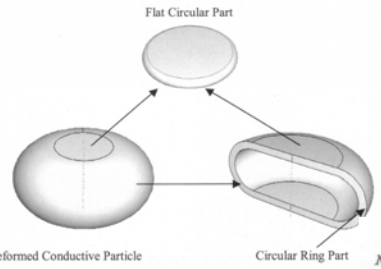

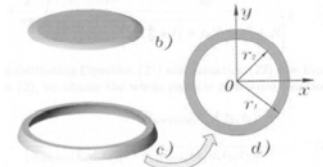

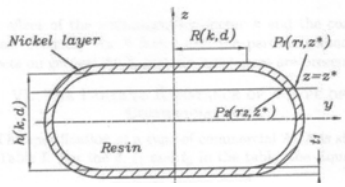

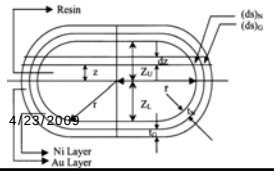

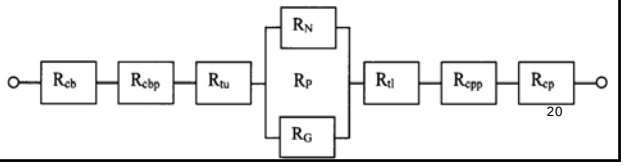

Agreement of models with experiment [Chin et al]

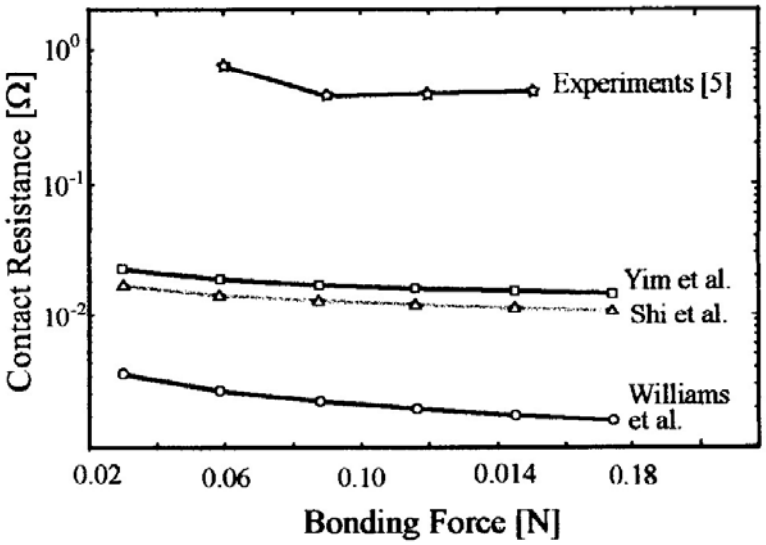

21

The Role of ACA/ACF Contraction Stress [Kwon et al (KAIST), ECTC'05]

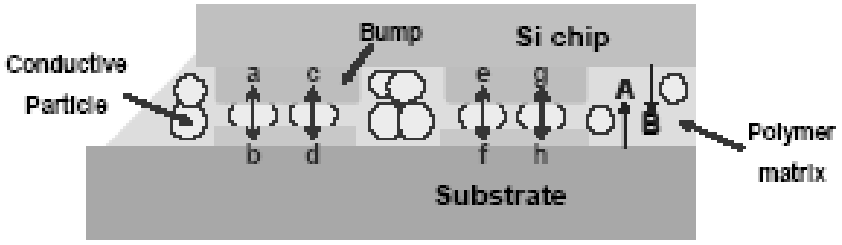

Figure 1. Schematics of conduction mechanism of ACFs flip chip joint. A and B: Contractive forces of ACFs, a-h: Repulsive forces of compressed conductive particles

4/23/2009

22

The Role of ACA/ACF Contraction Stress

[Kwon et al (KAIST), ECTC'05]

Increase in temperature in use relaxes contraction stress:

CTE & modulus

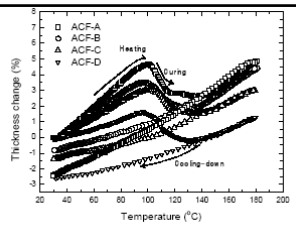

Figure 6. Dimensional changes of four ACFs along the thickness direction during curing and cooling-down processes

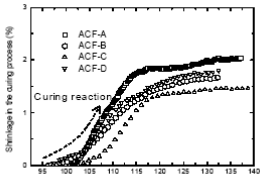

(a)

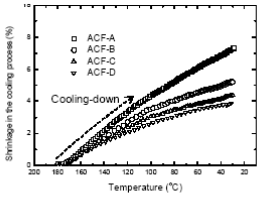

(b)

Figure 7. Shrinkage behaviors of four ACFs (a) during curing process and (b) during cooling-down process

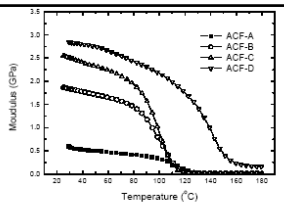

Figure 8. Modulus behaviors of cured ACFs during cooling-down to room temperature

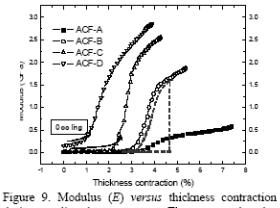

Figure 9. Modulus (E) *versus* thickness contraction ($d\varepsilon_z$) during cooling-down process. The area under the curve corresponds to the shrinkage stress

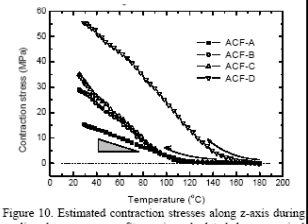

Figure 10. Estimated contraction stresses along z-axis during cooling-down process. Stress is calculated by numerical integration according to the equation (5)

ACA/ACF Contraction Stress [Chin et al]

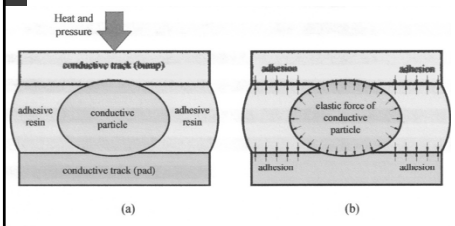

(a) (b)

Figure 3 Bonding process in ACA assemblies: a) loaded condition and b) unloaded condition. Deformation of the conductive tracks (bump and pad) is not shown for simplicity.

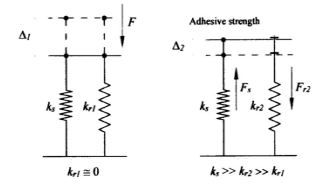

(a) (b)

Figure 4 One dimensional and pure elastic scheme of the interaction between forces and displacements during: (a) loaded condition and (b) unloaded condition.

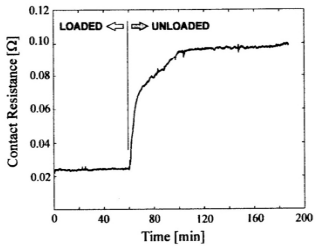

Figure 8 Contact resistance versus time obtained for sample #3 (resin #1, 60 min curi time)

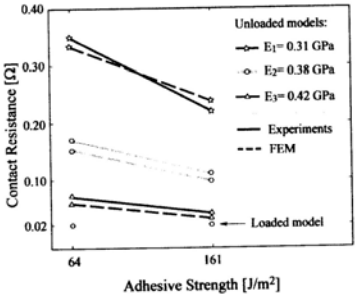

Figure 9 Contact resistance versus adhesive strength and modulus of elasticity. Experimental and numerical results are shown.

3 Electrical Properties: High-performance packages

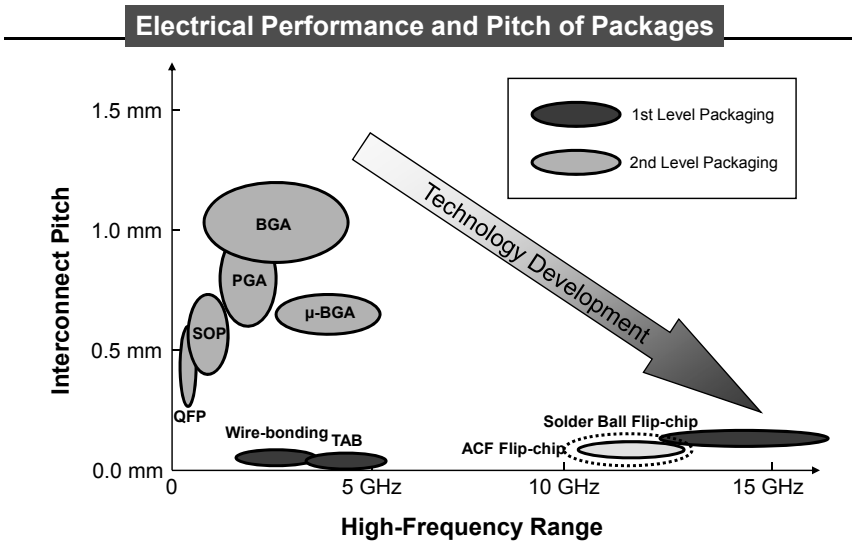

SOP : Small Outline Package

Test Chip and Board - Assembled DUT

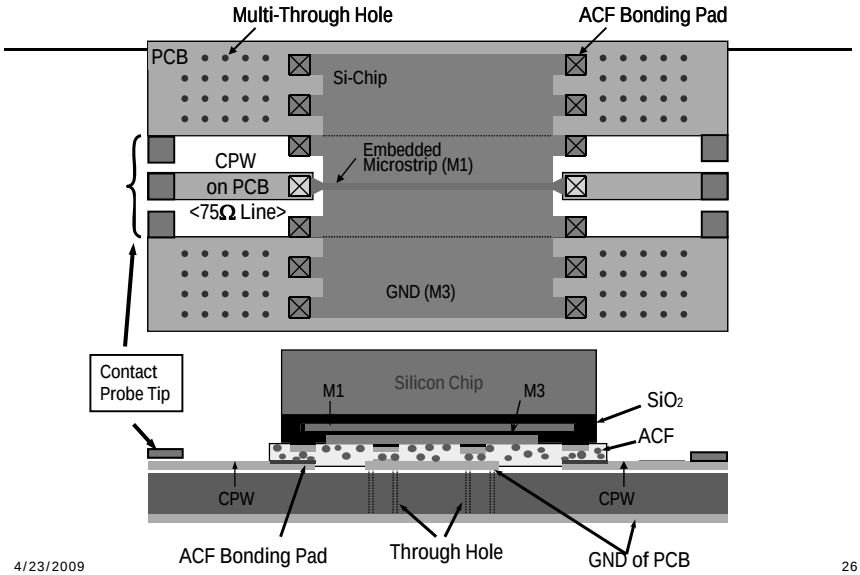

A comparison in transmission parameter of S21 between an ACA bonded and a solder bonded flip-chip interconnect

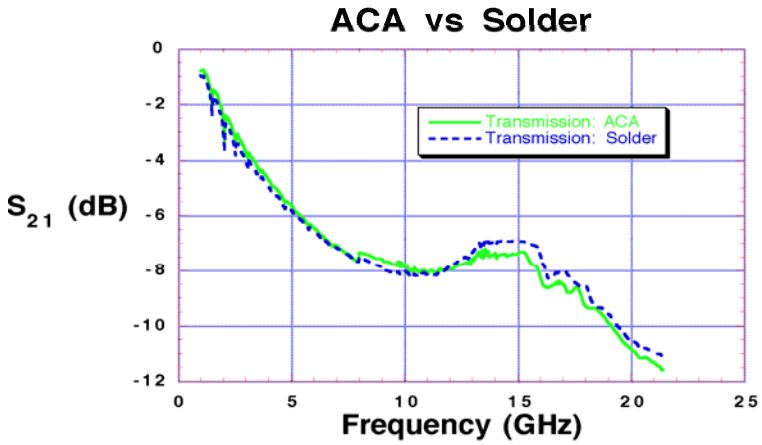

SPICE-Model for ACF Flipchip Interconnection (Paik et al)

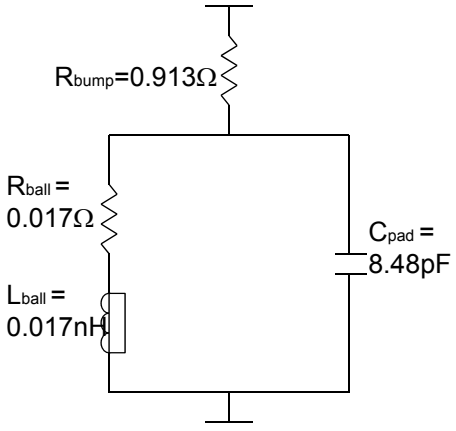

Measured Time-Domain Transmission through ACF

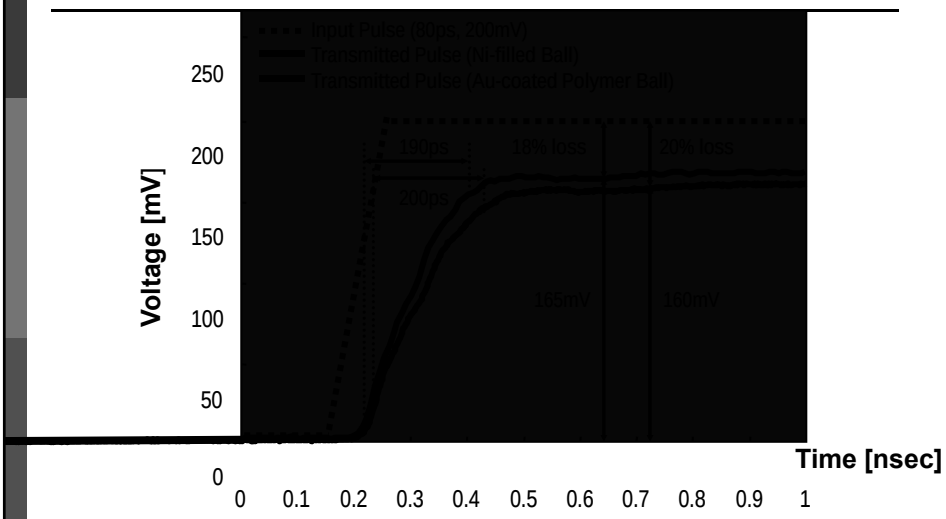

2.2 FEM Electrical Models: Solid & Coated Spheres

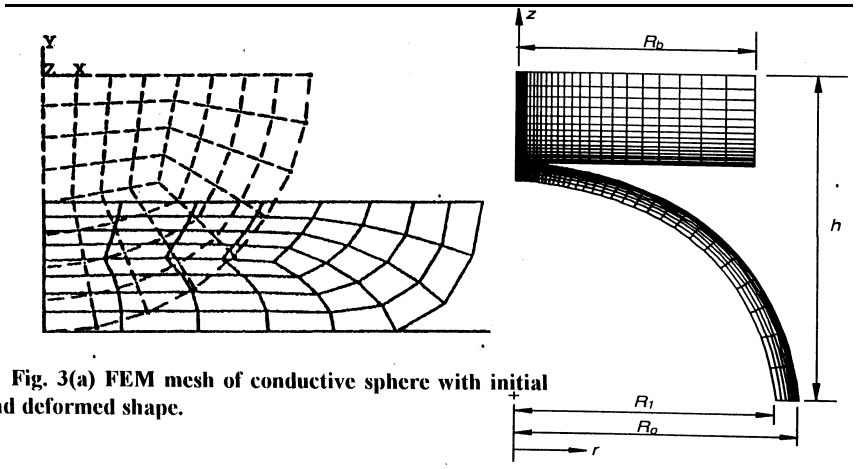

Fig. 3(a) FEM mesh of conductive sphere with initial and deformed shape.

Figure 4: *FE mesh of the metal-coated particle*

ACA: Particle Distributions

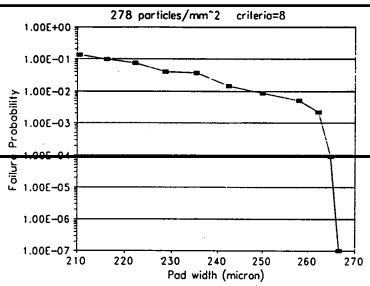

(b)

Figure 8.7: (a) The failure probability versus pad size for different particle densities for criteria = 3 & 8. (b) Expanded scales (failure probability versus pad size for 278/mm^2 and criteria = 8).

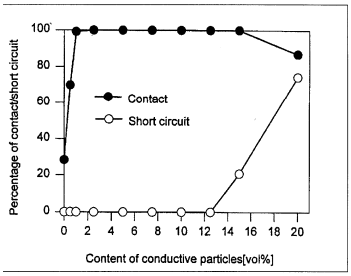

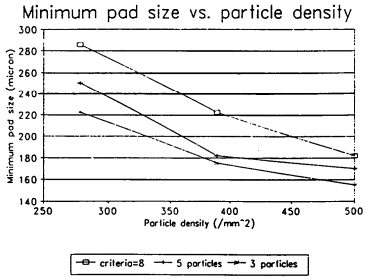

Figure 8.8: The minimum pad size versus particle loading density for different criteria.

Electrical Conductance Change with Particle Location

[Liu]

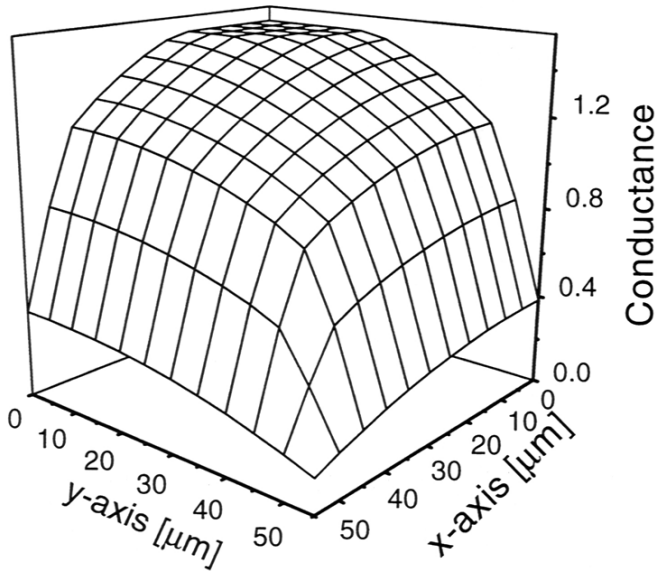

4.1 ACF TCE Reduction with fillers

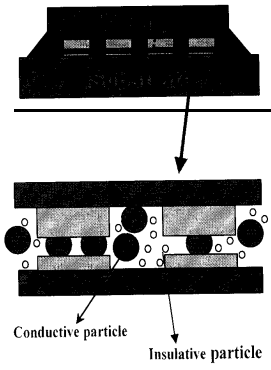

CTE (ppm / °C)	
Si chip	2.8
FR-4	18.0
Filled ACF:-	
10 % wt	42.9
30 % wt	35.2
50 % wt	28.0

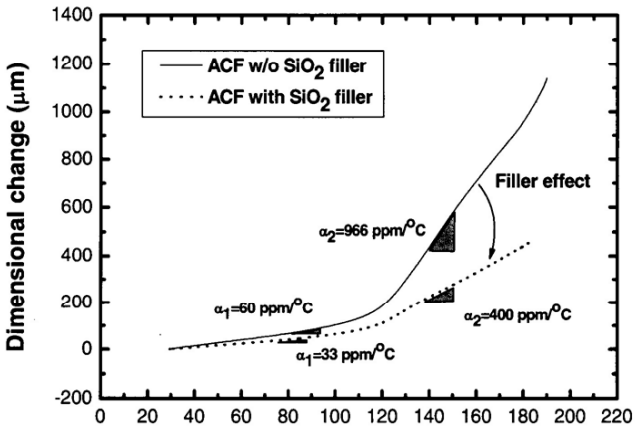

Effect of Fillers (Yim & Paik)

Effect of Fillers

(Yim & Paik)

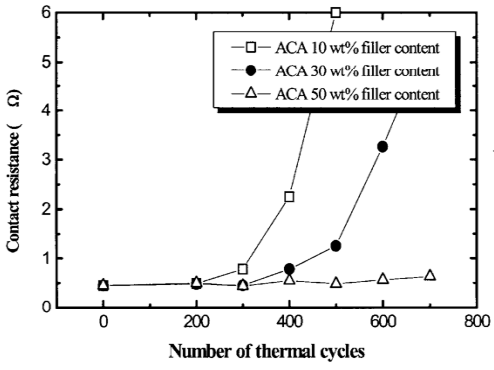

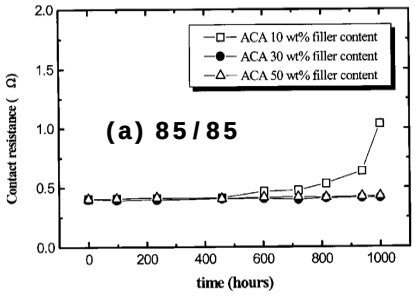

(a)

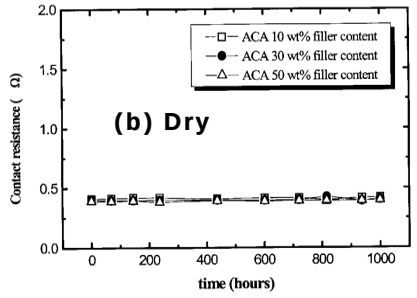

(b)

4.2 Thermal Conductivity

[Yim et al, ECTC'06]

ACP-3 has <1μm SiC filler added to Ni (ACP-1)

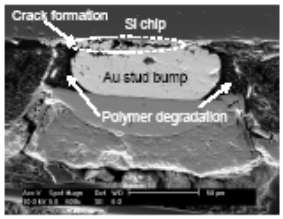

Fig. 6. Cross sectional SEM pictures at Au stud bumps joints by conventional ACA after current stressing reliability test.

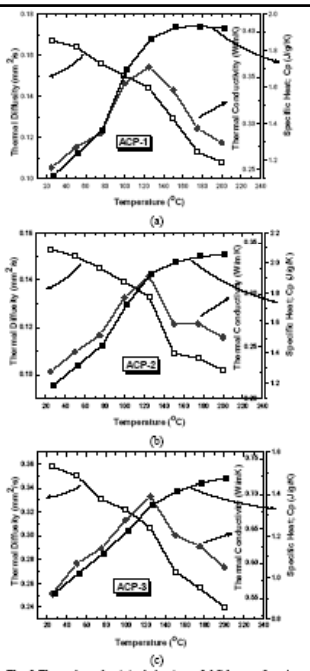

Fig. 2 Thermal conductivity behaviors of ACAs as a function of temperature for three ACA materials; (a) Ni-filled ACA, (b) Au-coated polymer ball-filled ACA and (c) Ni-filled and thermally conductive ACA.

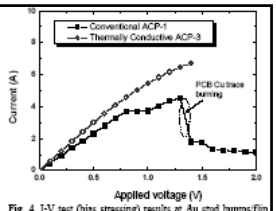

Fig. 4. I-V test (bias stressing) results at Au stud bumps/flip chip joints by conventional ACA and thermally conductive ACA.

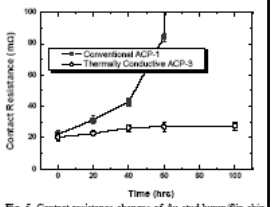

Fig. 5. Contact resistance changes of Au stud bump/flip chip joints using conventional ACA and thermally conductive ACA after 20, 40, 60, 100 hours under current stressing.

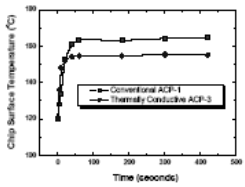

Fig. 7 Chip surface temperature of flip chip assemblies using conventional and thermally conductive ACAs as a function of current stressing time.

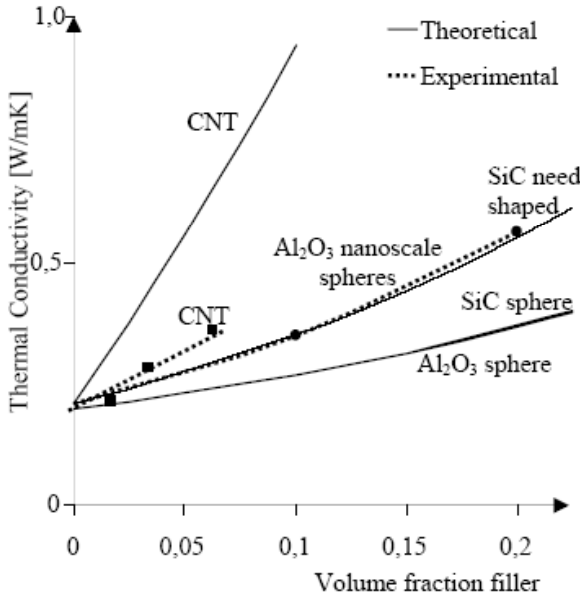

Fig. 4: Theoretical (according to Lewis-Nielsen theory [3]) and experimental values.

Epoxy thermal conductivity with fillers

(Ekstrand, Kristiansen, & Liu, ISSE 2005)

36

Anisotropic Conductive Adhesive (ACA) Enhancement

(Rongwei Zhang et al ECTC'08)

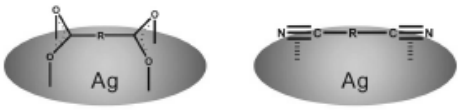

(A) (B)

Figure 5 Alignments of SAM1 and SAM2 on a submicron-sized Ag particle surface.

SAM-1:

"Molecular wires"
Oxide reduction
Lower resistance
Higher max current

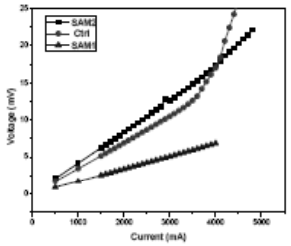

(a)

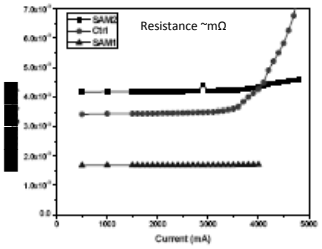

(b)

Figure 8 (a) I-V curve of ACA filled with Ag particles (Ctrl), SAM1-treated Ag particles and SAM2-treated Ag particles; (b) Corresponding I-R curves.

5. ACP Reliability

- Thermal cycling
- Flip-chip board warp
- Substrate Effects
  - Flip-chip on FR4
  - Co-planarity, etc
- Particle rupture
- Humidity testing

5.1 Daisy chain resistance values of flexible test circuits with various conductor metallizations bonded with Sn58Bi-filled ACA after temperature cycling from temperatures -40°C and +100°C (three hour cycle)

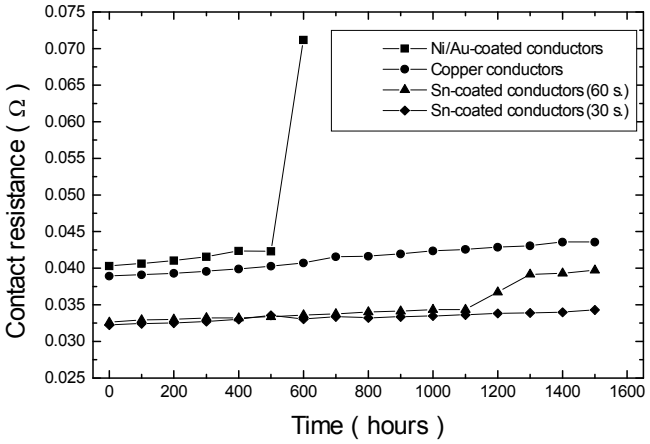

5.2 Flip-chip warpage

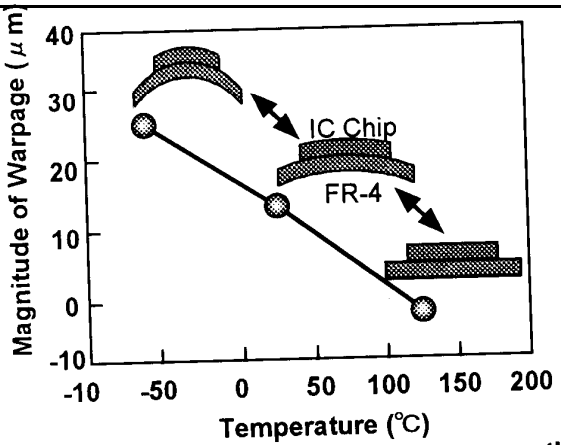

Figure 2. Influence of temperature upon the warpage of COB.

- Nagai et al, IEMT/IMC, 1999

Warpage increased by high CTE, Young's Modulus

(Cheng et al, IEEE Trans CPT 2006)

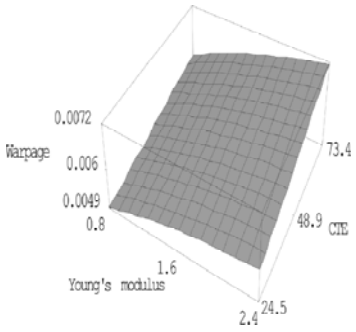

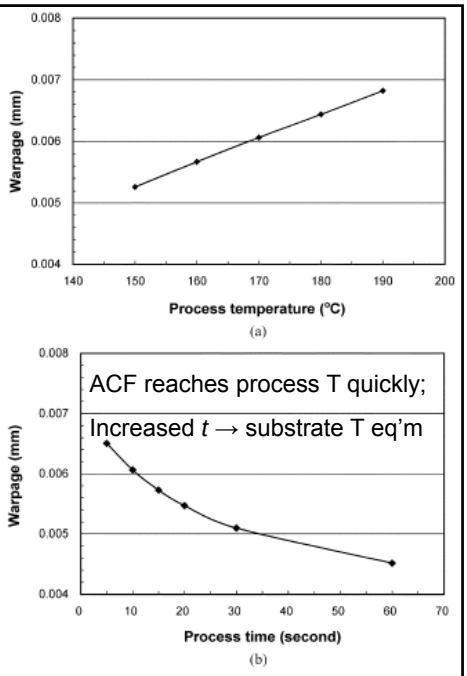

Fig. 15. Effect of process temperature and time: (a) process temperature and (b) process time.

4/23/2009

5.3 ACA Flip-Chip on FR4 & Flex

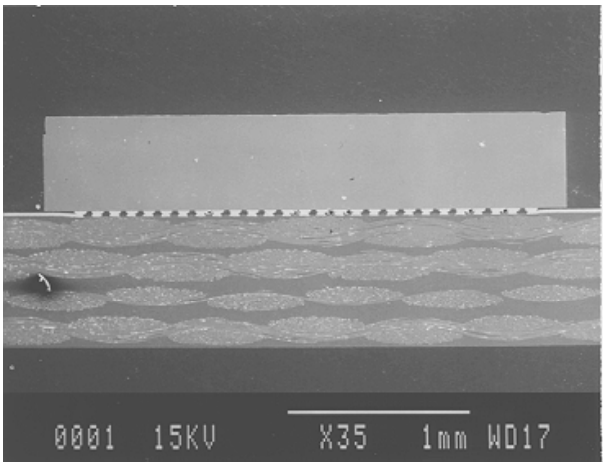

4/23/2009 42

ACA Contact R Variation on FR-4 [Liu et al]

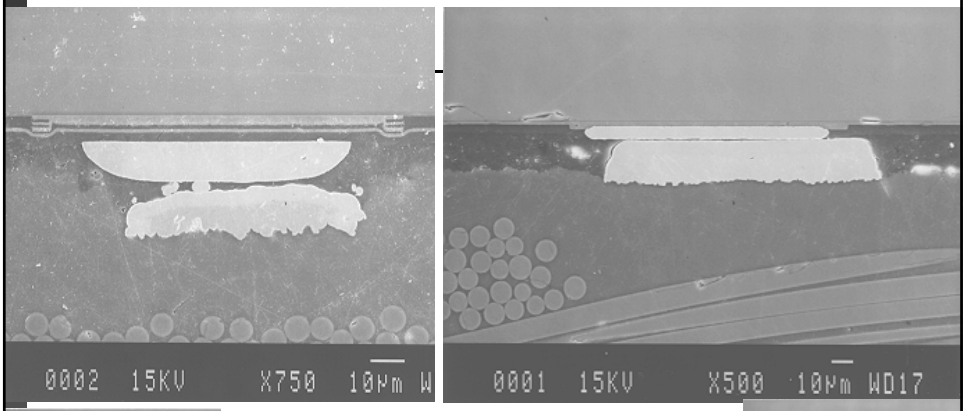

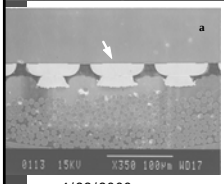

Resistances vary with pressure, which depends on position wrt glass fibers; (polymer softens)

ACA: Lu & Chen, Proc. ECTC 2008, pp. 1287-1293
ACA for Ultra-Thin Chip on Flex (UTCOF)

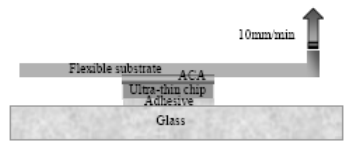

Fig. 4 Peeling test

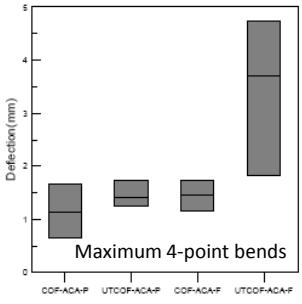

Maximum 4-point bends

4-point bending failures

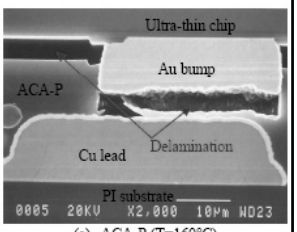

(a) ACA-P (T=160°C)

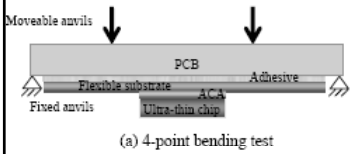

(a) 4-point bending test

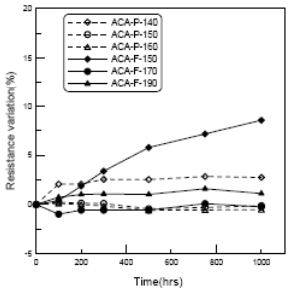

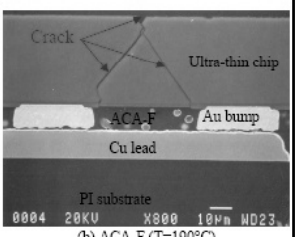

(b) ACA-F (T=190°C)

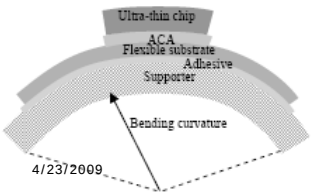

(b) static bending test

Static bend 30mm curvature

5.4 Particle Rupture

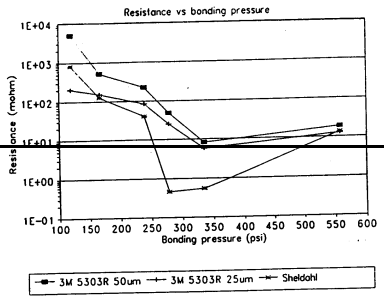

Figure 8.1: Resistance versus bonding pressure for the Cu(I) conductor for 3M material and Sheldahl material.

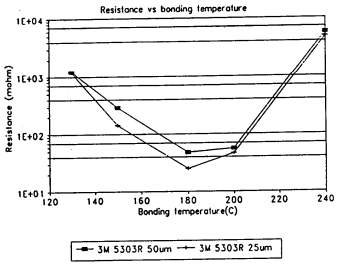

Figure 8.2: Bonding resistance versus bonding cure temperature for 3M material at 28

Particle Rupture

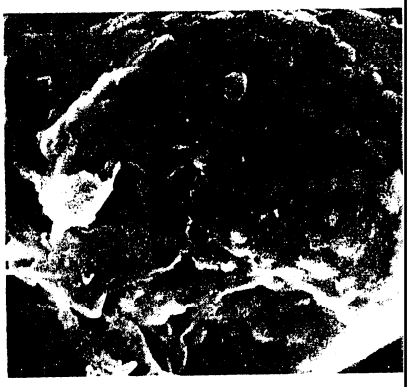

Before

After

Rupture/Resistance Modeling [Xie et al, ECTC'06]

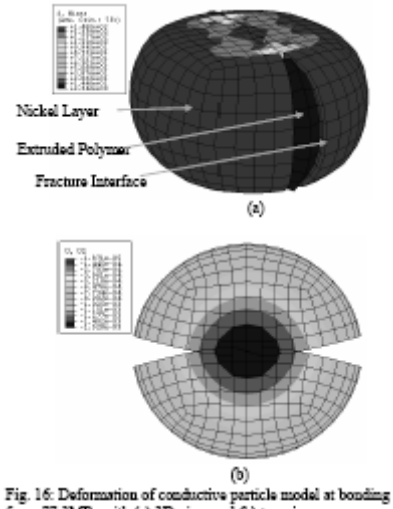

Fig. 16: Deformation of conductive particle model at bonding force 77.3MPa with (a) 3D view and (b) top view

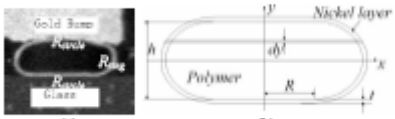

Fig. 17: (a) Components of particle resistance in a single particle and (b) profile of nickel coated polymer particle

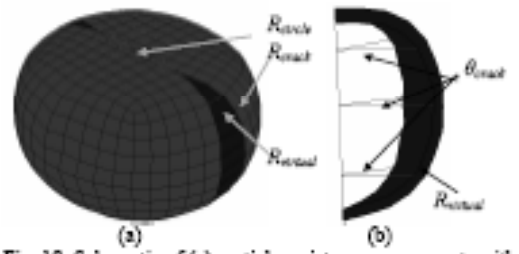

Fig. 18: Schematic of (a) particle resistance components with cracks and (b) virtual resistance

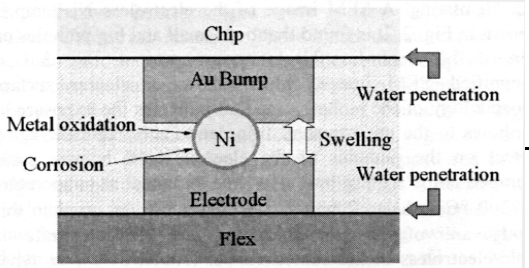

Figure 1. Typical degradation mechanisms in ACF joints.

5.5 ACF Humidity Failure

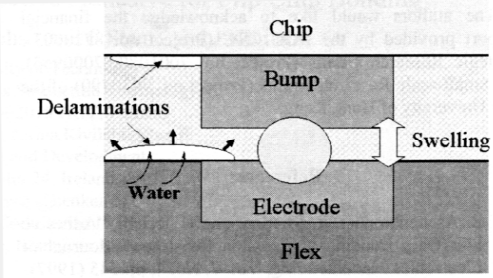

Figure 10. A schematic diagram showing the swelling of adhesive due to water absorption and swelling of delamination due to the water diffusion from flex.

4/23/2009

ACA Moisture [Ikeda et al]

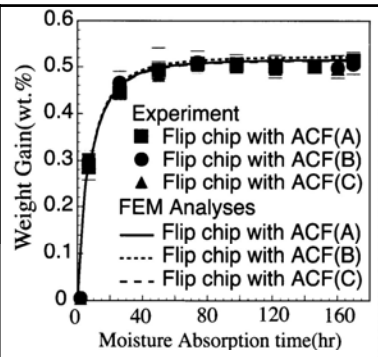

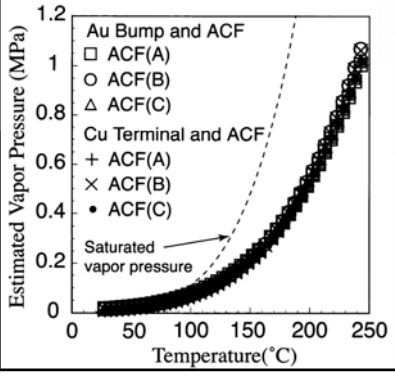

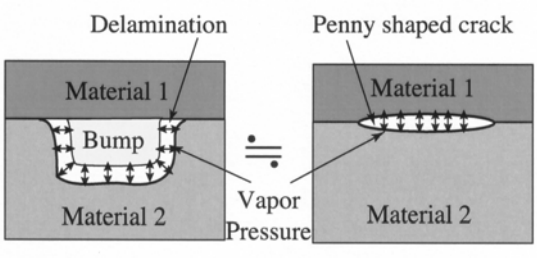

Fig. 11 Assumption of penny-shaped crack used in this study.

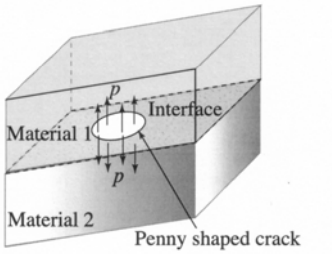

Fig. 12 Penny-shaped crack between dissimilar materials.

49

Moisture fails (Teh et al IEEE Trans CPT 2005)

MST JEDEC Level 2 Moisture sensitivity test 168hrs 85°C 60%RH + 3 x 240°C
PCT Pressure cooker test 144hrs 121°C 100%RH

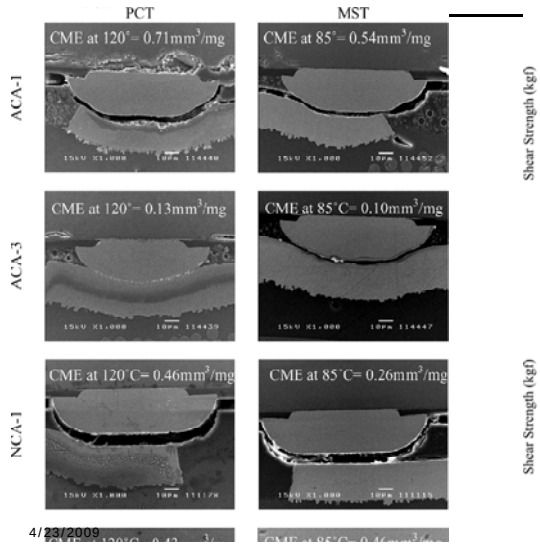

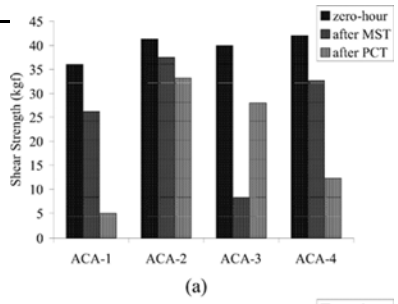

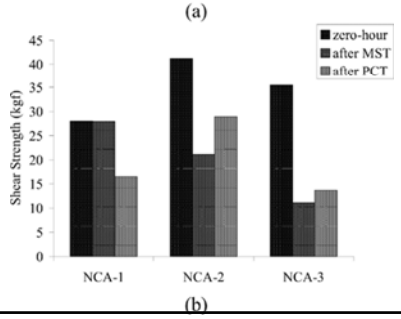

Hygroscopic swelling → bending, delamination

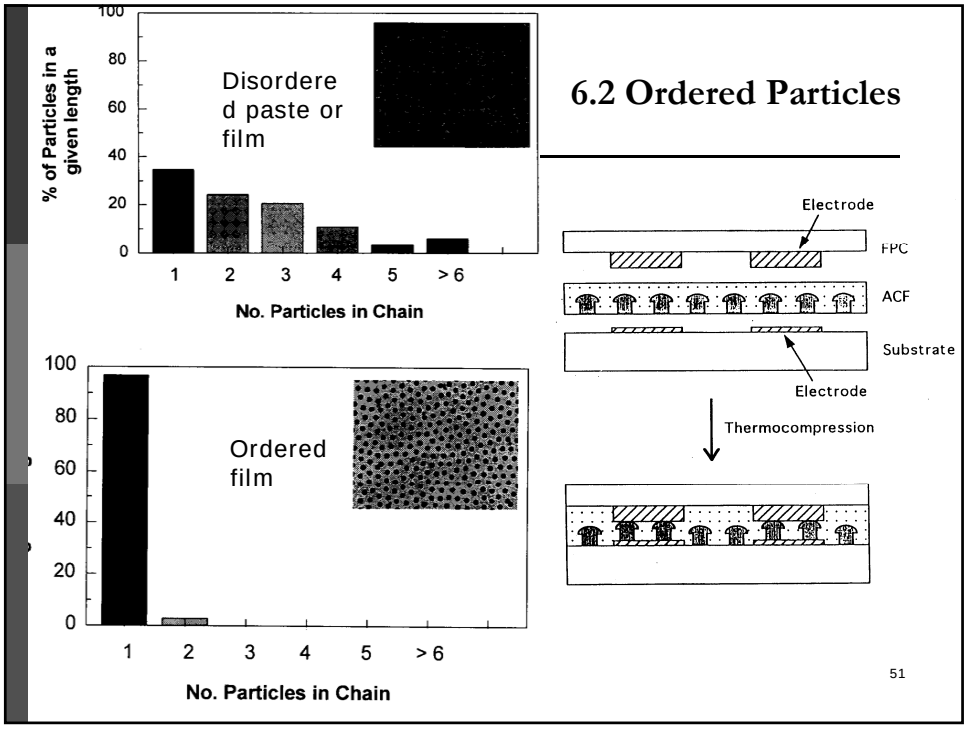
% of Particles in a given length
100
80
60
40
20
0
Disordered paste or film
1
2
3
4
5
> 6
No. Particles in Chain
100
80
60
40
20
0
Ordered film
1
2
3
4
5
> 6
No. Particles in Chain
6.2 Ordered Particles
Electrode
FPC
ACF
Substrate
Electrode
Thermocompression
51

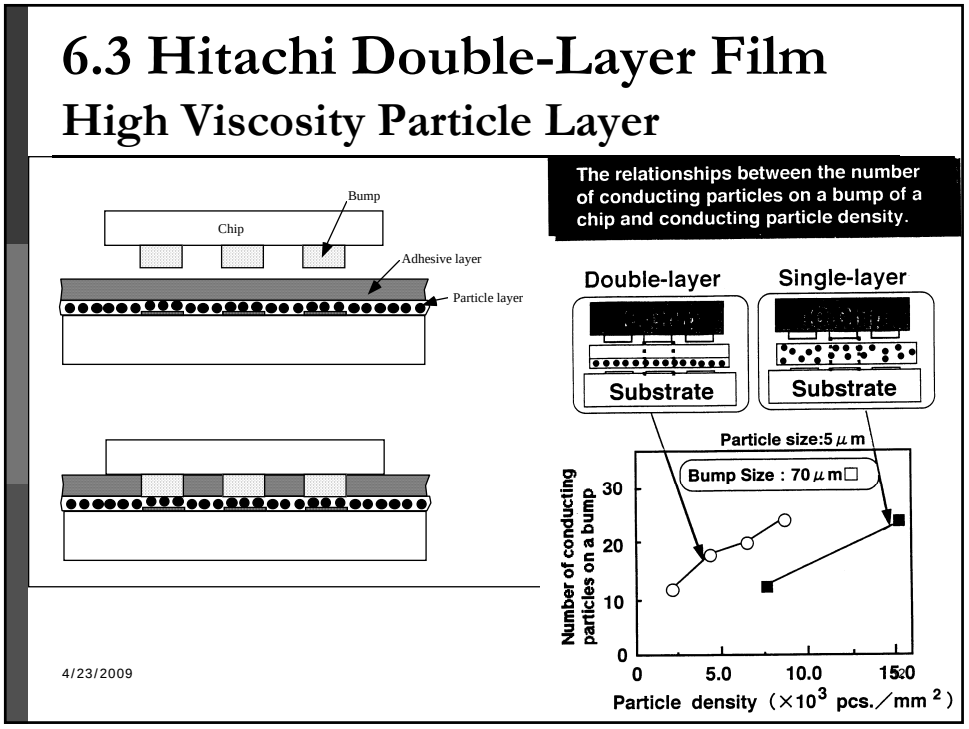
6.3 Hitachi Double-Layer Film
High Viscosity Particle Layer
Bump
Chip
Adhesive layer
Particle layer
The relationships between the number of conducting particles on a bump of a chip and conducting particle density.
Double-layer
Single-layer
Substrate
Substrate
Particle size:5 μm
Bump Size : 70 μm□
Number of conducting particles on a bump
30
20
10
0
0
5.0
10.0
15.0
Particle density (×10³ pcs./mm²)
4/23/2009

6.4 ACF Adhesive Thickness

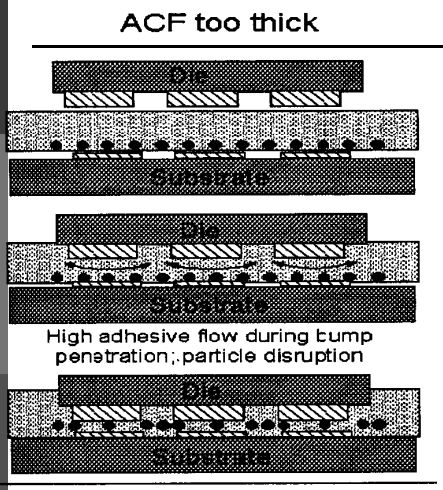

Figure 9. ACF thickness too large.

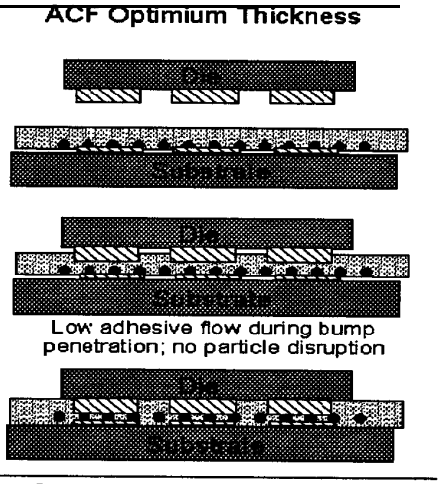

Figure 8. Optimised ACF thickness.